East Asian Monsoon Forcing and North Atlantic Subtropical High Modulation of Summer Great Plains Low-level Jet

Kelsey Malloy[1] and Ben P. Kirtman[2]

[1]Department of Applied Physics and Applied Mathematics, Columbia University
[2]University of Miami

December 7, 2022

Abstract

Dynamic influences on summertime seasonal United States rainfall variability are not well understood. A major cause of moisture transport is the Great Plains low-level jet (LLJ). Using observations and a dry atmospheric general circulation model, this study explored the distinct and combined impacts of two prominent atmospheric teleconnections - the East Asian monsoon (EAM) and North Atlantic subtropical high (NASH) - on the Great Plains LLJ in the summer. Separately, a strong EAM and strong western NASH are linked to a strengthened LLJ and positive rainfall anomalies in the Plains/ Midwest. Overall, NASH variability is more important for considering the LLJ impacts, but strong EAM events amplify western NASH-related Great Plains LLJ strengthening and associated rainfall signals. This occurs when the EAM-forced Rossby wave pattern over North America constructively interferes with low-level wind field, providing upper-level support for the LLJ and increasing mid- to upper-level divergence.

East Asian Monsoon Forcing and North Atlantic Subtropical High Modulation of Summer Great Plains Low-level Jet

Kelsey Malloy[1], **Ben P. Kirtman**[2,3,4]

[1]Department of Applied Physics and Applied Mathematics, Columbia University, New York, New York
[2]Rosenstiel School of Marine, Atmospheric, and Earth Science, University of Miami, Miami, Florida
[3]Cooperative Institute for Marine and Atmospheric Studies, University of Miami, Miami, Florida
[4]Institute for Data Science and Computing, University of Miami, Miami, Florida

Key Points:

- Variability of the Great Plains low-level jet is linked to the strength of the East Asian monsoon and North Atlantic subtropical high.
- North Atlantic subtropical high has a greater influence on the low-level jet and related rainfall, but the monsoon may amplify its impacts.
- Their interaction involves alignment of upper- and lower-level meridional wind anomalies, enhancing mid- to upper-level divergence.

Corresponding author: Kelsey Malloy, kmm2374@columbia.edu

Abstract

Dynamic influences on summertime seasonal United States rainfall variability are not well understood. A major cause of moisture transport is the Great Plains low-level jet (LLJ). Using observations and a dry atmospheric general circulation model, this study explored the distinct and combined impacts of two prominent atmospheric teleconnections – the East Asian monsoon (EAM) and North Atlantic subtropical high (NASH) – on the Great Plains LLJ in the summer. Separately, a strong EAM and strong western NASH are linked to a strengthened LLJ and positive rainfall anomalies in the Plains/ Midwest. Overall, NASH variability is more important for considering the LLJ impacts, but strong EAM events amplify western NASH-related Great Plains LLJ strengthening and associated rainfall signals. This occurs when the EAM-forced Rossby wave pattern over North America constructively interferes with low-level wind field, providing upper-level support for the LLJ and increasing mid- to upper-level divergence.

Plain Language Summary

Summer rainfall can greatly impact agriculture, and seasons with extreme wet or extreme dry conditions often harm human life and/or property. Therefore, it is important to understand fluctuations in seasonal rainfall and the dynamical processes involved. Moisture can be transported into the U.S. through a narrow belt of winds that peaks a few hundreds of meters above ground. We studied how the East Asian monsoon and a subtropical high system over the North Atlantic can impact this belt of winds and its related rainfall. When the North Atlantic subtropical high extends into the U.S., it strengthens the winds into the Plains and increases rainfall over the eastern U.S. A strong East Asian monsoon can amplify this response; this occurs because the monsoon triggers an atmospheric wave that crosses the North Pacific and North America, and its related flow in the upper levels can become in-phase with the belt of winds that is providing moisture to the Plains, amplifying processes that produce rainfall.

1 Introduction

Continental United States (CONUS) summer rainfall variability has implications for human health and the economy. Unfortunately, current subseasonal-to-seasonal forecasts for summer precipitation have relatively low skill (Becker et al., 2014; Hao et al., 2018; Jha et al., 2019; Slater et al., 2019; Malloy & Kirtman, 2020), likely because there is little to no consensus about the dominant cause(s) of low-frequency precipitation variability. Compared to winter, the warm season presents unique challenges, such as lower signal-to-noise ratios from weaker subtropical jet streams, SST anomalies, tropical convection systems, and extratropical circulation (Schubert et al., 2002; Dirmeyer et al., 2003; S. Zhou et al., 2012; Gianotti et al., 2013; Lee et al., 2009; Tian et al., 2017; Malloy & Kirtman, 2020).

The Great Plains low-level jet (LLJ) is a prominent circulation feature east of the Rocky Mountains, typically forming at nighttime just above the boundary layer between 925-850 hPa (Blackadar, 1957; Holton, 1967; T. Parish et al., 1988; Fast & McCorcle, 1990; Mitchell et al., 1995; Whiteman et al., 1997; Banta et al., 2002; Jiang et al., 2007; T. R. Parish & Oolman, 2010; Gimeno et al., 2016; Shapiro et al., 2016). Its fast-moving southerly winds act as a conveyor belt of heat and moisture to the Plains and Midwest, causing precipitation at the jet exit where low-level convergence occurs (Higgins et al., 1997; Weaver, Ruiz-Barradas, & Nigam, 2009; Pu & Dickinson, 2014; Hodges & Pu, 2019). Major pluvial events are linked to the strengthening of the Great Plains LLJ (Arritt et al., 1997; Cook et al., 2008; Feng et al., 2016) with low-level fluxes typically peaking in the mid-summer months (Weaver & Nigam, 2008); Algarra et al. (2019) found that the Great Plains LLJ contributes up to 70-90% of the moisture transport into the Plains and up to 50% of the moisture transport into the Great Lakes and northeast U.S. regions in the summer.

There are numerous large-scale influences on Great Plains LLJ strength and variability. Teleconnections, such as the Pacific-North America (PNA) pattern, are found to have strong links to LLJ strengthening (Harding & Snyder, 2015; Patricola et al., 2015; Mallakpour & Villarini, 2016; Weaver et al., 2016; Nayak & Villarini, 2017; Malloy & Kirtman, 2020). Anomalous ridging over the northeast Pacific and anomalous troughing over western North America – characteristics of a negative PNA – promote strengthening of low-level southerlies and enhanced moisture transport over the Plains.

Many studies have analyzed additional trans-Pacific upper-level wave patterns and their connections to U.S. hydroclimate variability. The Asia-North America (ANA) teleconnection, an upper-level height pattern initiated by East Asian monsoon (EAM) heating, has been shown to link the climate variability over Asia and North America (B. Wang et al., 2001; Lau & Weng, 2002; Zhu & Li, 2016, 2018; S. Zhao et al., 2018; Lopez et al., 2019; Malloy & Kirtman, 2022). The EAM has been shown to produce an equivalent barotropic wave train response with or without ENSO in the background state (Trenberth & Guillemot, 1996; Lau & Weng, 2002; Zhu & Li, 2016, 2018; Lopez et al., 2019). Like the PNA, the ANA pattern is associated with an anomalous trough over western North America, promoting Great Plains LLJ strengthening. Zhu and Li (2018) found the ANA relationship to boreal summer rainfall variability has become stronger in recent decades, likely due to a northward shift of the monsoon system closer to the East Asian jet.

The North Atlantic Subtropical High (NASH) has a prominent control over large-scale circulation and the Great Plains LLJ. The NASH experiences its own variability, with its westward expansion or shift linked to Plains and/or southeast U.S. hydroclimate (Ting & Wang, 2006; L. Li et al., 2012; Pu et al., 2016; Hodges & Pu, 2019; Wei et al., 2019; Nieto Ferreira & Rickenbach, 2020). Observational analysis and an associated GCM study suggested that Indian monsoon heating may result in increasing low-level easterly wind anomalies over the North Atlantic to shift the NASH westward (Kelly & Mapes, 2011, 2013). When the western ridge of the NASH intensifies, the Caribbean LLJ strengthens, increasing the easterly transport of moisture from the subtropical Atlantic and Caribbean Sea into the Gulf of Mexico (Mestas-Nuñez et al., 2007; C. Wang, 2007; Krishnamurthy et al., 2015; García-Martínez & Bollasina, 2020; Nieto Ferreira & Rickenbach, 2020). This additionally leads to increased southerlies in the Great Plains LLJ, enhancing the moisture fluxes into the Plains (T. R. Parish & Oolman, 2010; Algarra et al., 2019; Z.-Z. Hu et al., 2020). Nieto Ferreira and Rickenbach (2020) determined that western NASH events are associated with 40% greater Great Plains moisture transport compared to eastern NASH events. The NASH has shifted or extended west more frequently in recent decades, and it is projected that trend will continue in a warming climate (W. Li et al., 2011; L. Li et al., 2012; Tang et al., 2017), though changes may be seasonally dependent and also controlled by poleward or equatorward shifts (W. Zhou et al., 2021). Nevertheless, understanding the impacts from these changes may yield knowledge beyond seasonal or interannual timescales.

Lastly, sea surface temperature (SST) anomalies in both the Pacific and Atlantic have been linked to the summer LLJ on monthly timescales. A warm tropical and northern Pacific and cool north Atlantic are associated with the strengthening of the Great Plains LLJ (Ting & Wang, 1997; Weaver, Schubert, & Wang, 2009; Pegion & Kumar, 2010; Q. Hu & Feng, 2012; Veres & Hu, 2013; Yu et al., 2017; Danco & Martin, 2018), though the extent to which this relationship is dynamically driven has been disputed. For example, there is a strong intraseasonal and interannual condition to the link between El Niño-Southern Oscillation (ENSO) and the Great Plains LLJ strengthening (Krishnamurthy et al., 2015; Danco & Martin, 2018). Kam et al. (2014) and Malloy and Kirtman (2020) suggest that using tropical SST forecasts for long-range rainfall prediction may be limiting in the summer months. Atmospheric circulation variability (internal or forced) has been shown to exist in the absence of tropical forcing (A. Z. Liu et al., 1998; Ding et al., 2011; Schubert et al., 2011; Krishnamurthy et al., 2015; Zhu & Li, 2016; O'Reilly et al., 2018; S. Zhao et al., 2018) and may have a stronger link to Plains/Midwest hydroclimate (Schubert et al., 2002; Ding et al., 2011; Burgman & Jang, 2015; Patricola et al., 2015; O'Reilly et al., 2018; Malloy & Kirtman, 2020). In general, summer predictability beyond weather timescales has been related to the location and/or amplification of quasi-stationary Rossby waves (Ding & Wang, 2005; Schubert et al., 2011; Beverley et al., 2019, 2021; Mariotti et al., 2020). Agrawal et al. (2021) found that monsoon-forced teleconnections can help explain interannual variability of the Great Plains LLJ in May; a wave train that propagates over the U.S. can support favorable background states (i.e. enhanced differential heating over sloping terrain) for LLJ flow. Understanding the primary forcing mechanisms for these monsoon-forced planetary waves, such as from the EAM, and how they develop over North America during the summer season where influence from the NASH circulation is greatest, is essential. Therefore, this study will concentrate on atmospheric teleconnections active in the June-July-August (JJA) season, particularly the EAM's and NASH's relationship with the Great Plains LLJ.

Despite the considerable literature on the EAM and NASH and their distinct influence on CONUS rainfall variability, there is little to no exploration into how these teleconnections interact. Because the Great Plains LLJ is a key driver of summer precipitation, this study will investigate the Great Plains LLJ response to the EAM forcing and consider how the NASH modulates that response. Simple dry atmospheric general circulation models (AGCMs) have been successful in reproducing the dynamics and variability of quasi-stationary/planetary wave activity from diabatic heating related to monsoons (Zhu & Li, 2016, 2018; Lopez et al., 2019; Malloy & Kirtman, 2022). We will use a simple dry nonlinear AGCM to understand the large-scale responses and modulation of the Great Plains LLJ on seasonal-to-interannual timescales. Because the dry ACGM inputs surface temperature climatology, it does not simulate SST variability, effectively isolating the atmospheric teleconnection (EAM and NASH) impacts. Section 2 will describe the datasets, details of the nonlinear AGCM and the experiments, and the relevant analysis methods. Section 3 will present the results as follows: The observed responses of the EAM and NASH and their interactions will be quantified. Then, this paper will examine the AGCM's EAM-forced response of the Great Plains LLJ. Finally, we will evaluate how NASH modulates the EAM-forced response. Section 4 will serve as a summary and reflection of the results in the context of previous literature and future work needed.

2 Data and Methods

2.1 Observational Datasets

Pressure-level meridional wind, zonal wind, temperature, and geopotential height were taken from the European Centre for Medium-Range Weather Forecasts (ECMWF) fifth-generation reanalysis (ERA5). ERA5 atmospheric data is provided on a 0.25° latitude/longitude grid (Hersbach et al., 2020). U.S. precipitation data were taken from the CPC Unified Gauge-based Analysis, provided on a 0.25° latitude/longitude grid (Chen et al., 2008; Xie et al., 2007). This study used the June through August monthly data between 1979-2019 to serve as observations.

2.2 Model and Experiments

The model in this study is a dry, baroclinic, and nonlinear AGCM, i.e. it includes the full primitive equations of divergence, vorticity, temperature and surface pressure. It is a spectral model with Rhomboidal truncation at R42 – approximately 1.7° latitude by 2.8° longitude – with 26 vertical levels. The vertical levels are analogous to the Community Atmospheric Model, version 4 (CAM4), which uses hybrid sigma-pressure coordinate system. The AGCM is adapted from Brenner (1984) to remove moist processes.

Newtonian cooling is specified throughout the troposphere with enhanced damping near the surface. Rayleigh friction is specified at the lower levels and mimic realistic land-sea frictional contrasts to generate climatological features, such as the NASH, monsoonal systems, and the Great Plains LLJ. Realistic topography is also an important aspect of this model as the large-scale Great Plains LLJ requires topographical modulation of stationary flow (Byerle & Paegle, 2003; T. R. Parish & Oolman, 2010; Ting & Wang, 2006; Weaver & Nigam, 2011). Versions of this dry AGCM have been used in Kirtman et al. (2001) and is described in more detail in Malloy and Kirtman (2022). The AGCM has also been used by He et al. (2014) to diagnose Rossby wave generation in some climate sensitivity experiments and by Arcodia and Kirtman (2022) to examine the combined ENSO and MJO teleconnection. This simple, idealized model is used for evaluating the large-scale teleconnections, primarily quasi-stationary wave activity, and it exhibits simple dry dynamic processes.

The surface temperature climatology for JJA is input as background state for the model. This climatology was calculated from ERA5 data and interpolated to the model's grid. Each experiment was integrated forward for 900 days with the JJA background state to estimate the steady-state response for both seasonal and interannual analysis. Analysis excludes the first 100 days to assure that there is no contamination from the spin-up period.

This AGCM is used for both unforced and forced experiments. The unforced experiment, or control (hereby CTRL) run, is evaluated to compare climatology with observations. It is also compared to the EAM-forced runs to understand NASH modulation of the Great Plains LLJ, divergence, and circulation response in the model. The strong EAM experiment applies a constant diabatic heating via Gaussian bubble with a maximum of 2 K day^{-1} centered at 30°N, 120°E and 300 hPa (see Supplementary Figure 1), similar to Zhu and Li (2016) and identical to Malloy and Kirtman (2022). The weak EAM experiment applies a forcing in the same location and of the same magnitude, but with the opposite sign i.e. there is negative diabatic heating (or cooling).

2.3 Analysis Methods

To investigate the separate and combined roles of the EAM and NASH in both observations and the AGCM, we calculated difference composites of 900-hPa meridional wind (V900) anomalies, 250-hPa geopotential height (Z250) anomalies, and rainfall anomalies. This means that anomalies are averaged for upper tercile events, and then subtracted from anomalies averaged from lower tercile events. We chose a composite analysis to highlight any nonlinearities in responses as weak and strong events may not yield equal and opposite LLJ anomalies. The EAM index is defined by 200-hPa zonal wind (U200) circulation as described in G. Zhao et al. (2015): U200(2.5-10°N,105-140°E) – U200(17.5-22.5°N, 105-140°E) + U200(30-37.5°N,105-140°E), where U200 is averaged anomalies within the domain in the parentheses. The western NASH index is defined as follows: Z850(15-28°N, 50-85°W). A variation of this intensity index was used by L. Li et al. (2012) and Nieto Ferreira and Rickenbach (2020) in evaluating Z850 anomaly fields associated with the Great Plains LLJ strengthening, but this index highlights northern NASH variability, which impacts Plains/Midwest rainfall variability to a greater extent. Overall, the index distinguishes between strong western NASH events, with the western ridge over North America, and weak western NASH events, with the western ridge remaining over the Atlantic (cf. Figure 1g-i, purple vs. green contours). All indices are standardized before anomalies are composited. We also composited the 1560 geopotential meter (1560-gpm) lines for observations corresponding to the strong and weak events to signify the NASH extent (W. Li et al., 2011) for the samples.

In addition, these composites are organized by a secondary condition, e.g. western NASH-related anomalies are further differentiated by strong (upper tercile) or weak (lower tercile) EAM events before averaging. To assess the significance of these difference composites, we performed a two-sided Wilcoxon rank-sum test. This test is preferred because it does not assume a Gaussian distribution, but it compares two samples' population mean ranks by considering if their distributions are the same.

To understand potential processes associated with these difference composites in observations and CTRL experiment, we included composites of meridional wind anomaly profiles averaged between 25-30°N, the latitude where the Great Plains LLJ and its related V900 anomalies are located. These composites separate by weak/strong western NASH and weak/strong EAM. This aids in visualizing the interactions in the vertical.

Finally, we assessed NASH's influence on the EAM-forced responses in the dry AGCM using difference of the composites, i.e. strong – weak EAM response during strong western NASH events minus strong – weak EAM response during weak western NASH events. This determines whether the dry AGCM can simulate the correct tendency of the response by NASH modulation. Anomalies are calculated by subtracting the climatology from the CTRL experiment, and weak/strong western NASH events are based on the lower/upper quintile thresholds calculated from the CTRL experiment.

3 Results

3.1 Observed Conditional Composite Analysis

Figure 1 and Figure 2 decompose the separate and combined influences of the EAM and NASH teleconnections in ERA5. The strong – weak western NASH difference composites in Figure 1a-c indicate that a western NASH is related to a 1-1.5 m s^{-1} strengthening of the Great Plains LLJ (Fig. 1a) and up to 1 mm day^{-1} rainfall anomalies over most of the eastern U.S. (Fig. 1b). The strong western NASH events (purple contour) correspond with a 1560-gpm line that extends far into the Gulf States, consistent with previous literature that connects west NASH extensions or shifts with amplified LLJ-related rainfall (W. Li et al., 2011; L. Li et al., 2012). There is also an anomalous ridge-trough pattern oriented west-east over North America (Fig. 1c).

When considering the strength of the EAM, the anomalous circulation and rainfall discussed above varies. Difference composites evaluated during weak EAM events (Figure 1d-f) show a southward-shifted Great Plains LLJ that does not extend far into CONUS (Fig. 1d). Rainfall anomalies of $\sim$1.5-2 mm day^{-1} are found over the Gulf States only, with dry anomalies over parts of the Plains/Midwest (Fig. 1e). In contrast, during a strong EAM (Fig. 1g-i), the Great Plains LLJ strengthening is greater ($>$2 m s^{-1}) and penetrates further into the U.S. (Fig. 1g). This is related to more extreme wet anomalies ($>$2 mm day^{-1}) stretching from the Plains to the Northeast U.S. The NASH-related Z250 anomalies are different between weak and strong EAM events (Fig. 1f,i), particularly over East Asia, North America, and the North Atlantic. The north-south orientation of anomalous trough-ridge pattern over CONUS during strong EAM events signals a negative PNA and enhanced meridional transport (Harding & Snyder, 2015; Malloy & Kirtman, 2020).

We considered the reverse analysis as well by taking strong – weak EAM difference composites of V900 anomalies, further separated into weak or strong western NASH events, as seen in Figure 2. A strengthened EAM is associated with a $\sim$0.5 m s^{-1} strengthening of the Great Plains LLJ (Fig. 2a), though is further east from the Rockies than the climatological Great Plains LLJ location and the NASH-related LLJ strengthening. Rainfall anomalies are modest – up to 0.75 mm day^{-1} – in the northern Plains and into Canada (Fig. 2b). An anomalous ridge is stretched over the North Pacific at around 30°N with an upper-level wave pattern emanating northward over East Asia (Fig. 2c). In addition, there is a general southwest-northeast pattern of an anomalous trough-ridge over North America, and an anomalous trough off the coast of Northeast U.S.

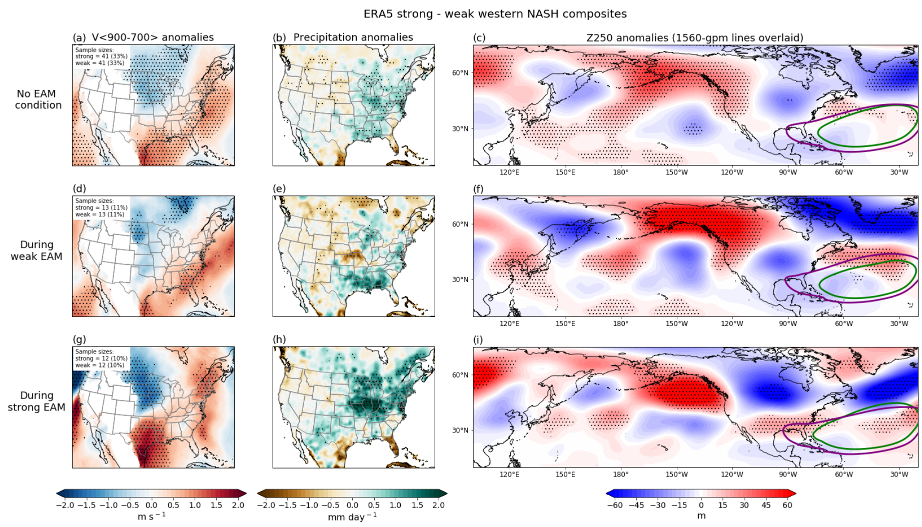

Figure 1. ERA5 strong – weak western NASH difference composites (a-c) with no EAM condition considered, (d-f) only during weak EAM events, and (g-i) only during strong EAM events. Difference composites of (a,d,g) V900 anomalies, (d,e,h) CPC gauge-based precipitation anomalies, and (c,f,i) Z250 anomalies, with purple and green contours denoting the 1560-gpm line for strong and weak composites, respectively. Sample sizes for the composites and the percentage of total events the samples represent are annotated on top left of each row. Stippling indicates anomalies significant at 90% confidence level based on the Wilcoxin rank-sum test.

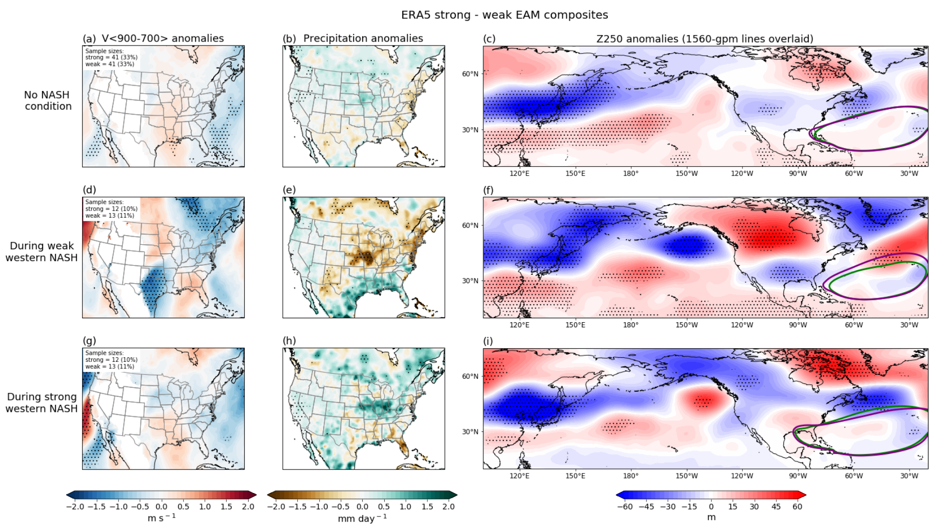

Figure 2. Similar format as Fig. 1, but ERA5 strong – weak EAM difference composites (a-c) with no NASH condition considered, (d-f) only during weak western NASH events, and (g-i) only during strong western NASH events.

Difference composites taken during weak western NASH events (Fig. 2d-f) reveal $\sim$1.5 m s^{-1} weakening of the Great Plains LLJ (Fig. 2d) and $\sim$2 mm day^{-1} dry anomalies over the Plains, Midwest, and Northeast U.S. (Fig. 2e). During strong western NASH events (Figure 2g-i), the Great Plains LLJ strengthening is weakly positive but not statistically significant (Fig. 2g), and there are ∼1-1.5 mm day^{-1} wet anomalies (Fig. 2h). The greatest differences in upper-level wave pattern are seen over the eastern North Pacific and North America, with opposite patterns depending on western NASH strength. This suggests that NASH exerts the primary influence over the Great Plains LLJ regardless of the EAM strength. In addition, because the anomalies are only statistically significant during weak western NASH events, EAM-related wave patterns may destructively interfere with strong western NASH-related wave patterns.

To further understand processes between the strong and weak events, Figure 3 shows the vertical profile of meridional wind anomalies averaged between 25-30°N. Rows differentiate between NASH strength, and columns differentiate between EAM strength. The EAM-related flow can be discerned east of the Himalayas (100-120°E) by the northerlies (Fig. 3a,c) or southerlies (Fig. 3b,d), which signals whether there is low-level divergence or convergence over the EAM region, respectively. The Great Plains LLJ is found between -100 and -90°W, with northerlies coinciding with a weak western NASH (Fig. 3a,b) and southerlies coinciding with a strong western NASH (Fig. 3c,d). During weak EAM and weak western NASH events (Fig. 3a), as well as during strong EAM and strong western NASH events (Fig. 3d), the LLJ-related winds are of the same sign as the upper-level flow. This suggests that when the EAM and western NASH are both weak or strong, their related circulation patterns are in constructive interference, i.e. the low- and upper-level flow are in alignment to promote enhanced precipitation patterns. This alignment of the meridional wind anomalies does not occur when the EAM is strong and the western NASH is weak, or vice versa (Fig. 3b,c).

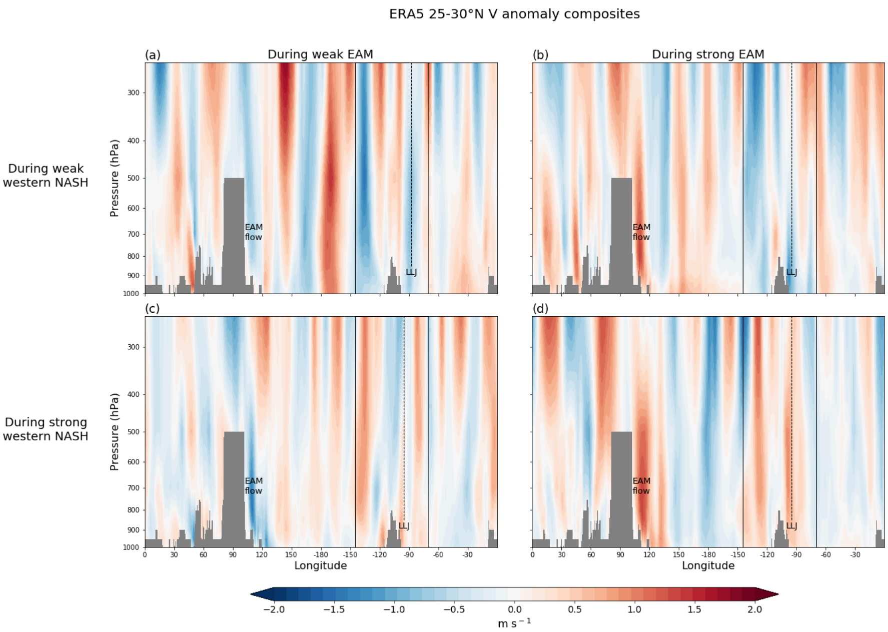

Figure 3. ERA5 composites of V anomaly vertical profiles averaged between 25-30°N during (a) weak western NASH and weak EAM events, (b) weak western NASH and strong EAM events, (c) strong western NASH and weak EAM events, and (d) strong western NASH and strong EAM events. Each panel annotates the approximate location of EAM-related flow and the Great Plains LLJ, and a thin vertical dotted line from LLJ is displayed to visualize upper-level support (or lack thereof).

While the idea that monsoon-forced teleconnections can influence low-level flow and related precipitation is supported by previous literature (Harding & Snyder, 2015; Mallakpour & Villarini, 2016; Agrawal et al., 2021; Malloy & Kirtman, 2022), we recognize the small sample sizes of the difference composites from the observational dataset. Therefore, in the next part of this study, we explore whether a simple dry AGCM can reproduce this interference between the EAM and NASH in influencing the Great Plains LLJ. In addition, it might be possible that a common driver, like ENSO, is modulating EAM-NASH interactions. Though we inspected the months that went into each composite and did not note any composites or phase of EAM/NASH that heavily favored an ENSO phase (see Supplementary Table 1), it would be advantageous to use the dry AGCM since it does not simulate SST variability and hence we can isolate the atmospheric influence.

3.2 Control Experiment Climatology and Biases

Before analyzing the dry AGCM responses, we evaluated the climatological biases of the model and its ability to produce realistic dynamic responses (e.g. quasi-stationary Rossby waves). Zonally-asymmetric components (represented by *) of time-mean circulation (represented by $\bar{\ }$) – also known as stationary waves – are useful for understanding the production and maintenance of Rossby waves. Seasonally, stationary waves describe preferred locations of meridional fluxes of heat and moisture, affecting hydroclimate. We compared the stationary waves in ERA5 and the CTRL experiment (no heating forcing) from the dry AGCM (Figure 4). In observations, $\overline{Z250'}^*$ generally features high pressure over the continents and low pressures over the ocean basins in the midlatitudes and subtropics at the edge of the East Asian or North Atlantic jet (Fig. 4a). The CTRL experiment exhibits similar patterns (Fig. 4b) but with biases over the Pacific and Atlantic (Fig. 4c). The bands of low pressure are higher in latitude over the Pacific, and the Atlantic is missing a band of low pressure at the subtropics. This has implications for the location of jet streams; the CTRL experiment $\overline{U250}$ bias (overlaid on Fig. 4c) indicates a jet stream shifted northward. Overall, the model captures basic characteristics of upper-level circulation, but these biases are important for understanding the production of Rossby wave responses in the forcing experiments.

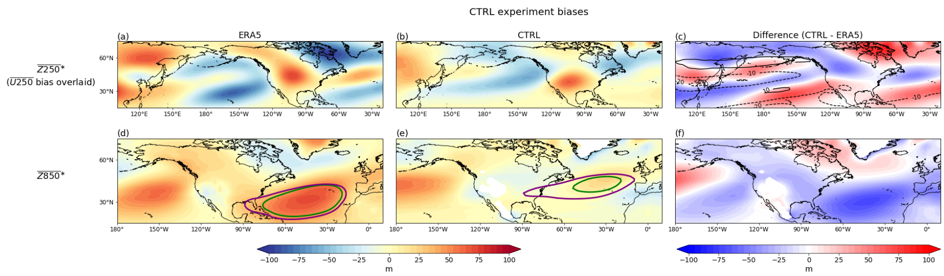

Figure 4. (a-c) Zonally-asymmetric component of the Z250 climatology for (a) ERA5, (b) CTRL experiment, and (c) the subtraction difference between CTRL experiment and ERA5, with the U250 climatological bias overlaid (black contours). (d-f) Same as top row, but for Z850. The purple and green contours denote the 1560-gpm line for the strong and weak NASH events, respectively, for both (d) ERA5 and (b) CTRL experiment.

$\overline{Z850'}^*$ from observations presents high pressure systems over the ocean basins (Fig. 4d), which coincides with the climatological location of subtropical highs (e.g. NASH). These ridges generally appear in the CTRL experiment (Fig. 4e), but the NASH is weaker and further north. These biases may have implications for discerning NASH influences, e.g. related anomalies that are higher in latitude than observations. Nevertheless, NASH variability is simulated in this model, as seen by comparing the composited positive and negative western NASH events between ERA5 and CTRL experiment (purple and green contours in Fig. 4d,e). The dry AGCM simulates strong western NASH events with western ridge extensions over CONUS and weak western NASH events with western ridge extentions that remain over the Atlantic, though the NASH extents are generally further north and exhibit greater variability between the weak and strong events. Overall, the basic NASH circulation and variability and its connection to the Great Plains LLJ is represented.

V900 climatology, which indicates the Great Plains LLJ climatology, can be compared in Figure 5. The ERA5 time-mean V900 shows a strong ($\sim$8 m s^{-1}) Great Plains LLJ feature (Fig. 5a). Despite the climatological core being about 5° northward from observational estimates, the location of the Great Plains LLJ in CTRL experiment is close to the Rockies, and general V900 circulation features over East Asia, North Pacific, and North America are represented in the model despite a northward-shifted bias. The magnitude of the climatological core is 3 m s^{-1}, which is weaker than the observations. However, the objective of the study is to analyze large-scale dynamical differences between forced experiments, not to represent thermodynamics, diurnally-varying radiative processes, nor mesoscale physics; therefore, this simulated Great Plains LLJ is within reason given that the model has relatively coarse resolution and lacks moist processes and associated land-atmosphere feedbacks.

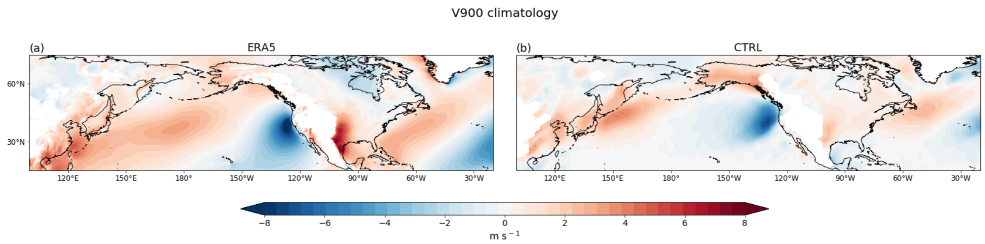

Figure 5. V900 climatology for (left) ERA5 and (right) CTRL experiment.

3.3 Strong – Weak EAM-forced Experiment Analysis

An advantage of this experiment setup with the dry nonlinear AGCM is that one can assess the effect of sub-sampling 90-day (or one single season) means during the 900-day experiment. Figure 6 demonstrates the internal variability of 90-day V900 means for this experiment; for V900 responses, the σ values are relatively large on the northern and southern edges of the climatological Great Plains LLJ region, and substantial off both North American coasts. This suggests that fluctuations in V900 are primarily at the northern edge of the climatological LLJ. The Z250 and Z850 responses indicate relatively higher σ values along the approximate climatological jet stream latitude and along the boundaries of climatological subtropical highs, respectively (Figure 7). This likely means that fluctuations in upper and lower heights are linked to East Asian jet variations and shifts in the subtropical highs, respectively. By dividing the time-mean difference by this standard deviation, we assess the robustness (or statistical significance) of the long-term response on seasonal-to-interannual timescales.

The EAM-forced V900 response is summarized in Figure 8, indicating a 0.5-1 m s^{-1} strengthening – a $\sim$25% magnitude increase compared to Figure 5b – in the Great Plains LLJ. This strengthening is confined to the northern side of the jet (Fig. 8c), which differs from the strong – weak EAM difference composite in Figure 2a. Overall, this forced

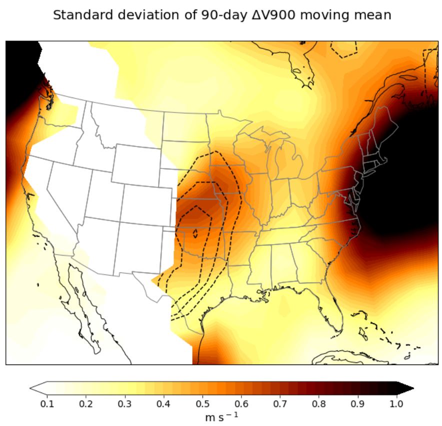

Figure 6. Standard deviation of the 90-day ΔV900 (Δ = strong EAM experiment - weak EAM experiment) moving mean. Climatological Great Plains LLJ is overlaid (black dashed contours).

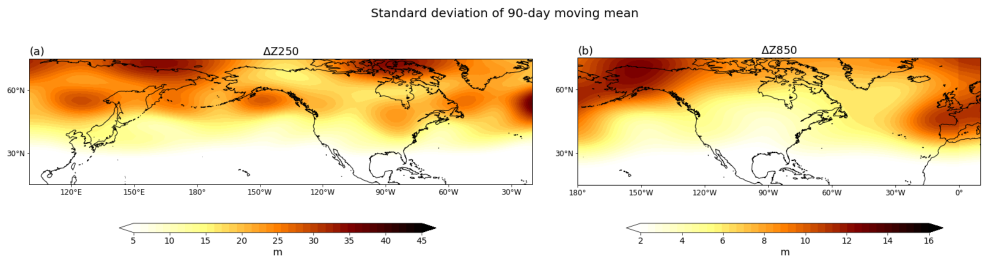

Figure 7. Standard deviation of the 90-day (left) ΔZ250 and (right) ΔZ850 moving mean.

response is considered robust on the seasonal timescale in the Great Plains and over the Gulf of Mexico, seen by the positive (negative) difference values that exceed 1σ (-1σ).

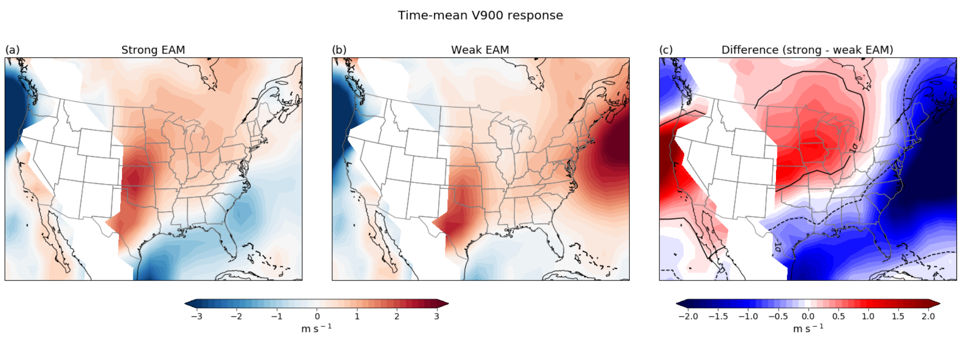

Figure 8. Time-mean V900 climatology for (a) strong EAM experiment and (b) weak EAM experiment. (c) Subtraction difference between strong EAM experiment and weak EAM experiment time-mean V900, with the 1σ (solid black) and -1σ (dashed black) contours overlaid by dividing difference by the standard deviation of the 90-day ΔV900 moving mean.

The EAM Z250 time-mean response shows zonally-oriented troughs and ridges that stretch from the EAM region and over the North Pacific (Figure 9a), with an anomalous trough-ridge pattern oriented west-east over North America, similar to the observed pattern (cf. Figure 2c). The anomalous trough over western North America is typically associated with Great Plains LLJ strengthening (Harding & Snyder, 2015; Mallakpour & Villarini, 2016; Malloy & Kirtman, 2020). The EAM Z850 time-mean response (right) presents anomalous ridging over much of the North Pacific and North America and anomalous troughing over the mid-latitude Atlantic, which could signal an increased variability of the NASH in the west-east direction. The Z250 and Z850 responses are mostly robust except for the high latitudes and the eastern North Pacific/Alaska region.

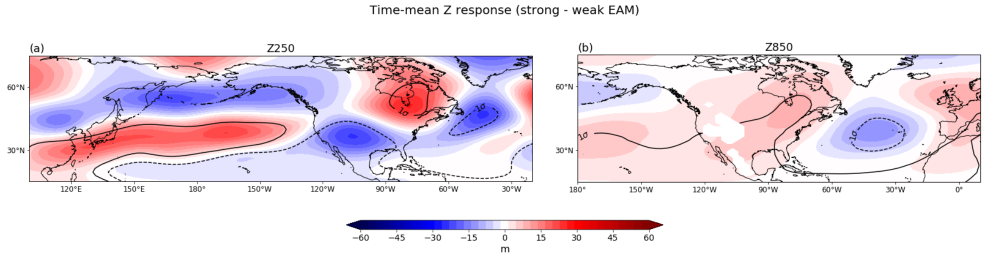

Figure 9. Subtraction difference between strong EAM experiment and weak EAM experiment zonally-asymmetric component of the time-mean (a) Z250 and (b) Z850. The 1σ (solid black) and -1σ (dashed black) contours are overlaid as in Fig. 8.

To get a sense of the response in the vertical, we assessed the latitudinally averaged cross-section of strong – weak EAM meridional wind (V) and divergence response in the general region where the downstream wave response travels (35-45°N; Figure 10). The response is mostly equivalent barotropic except for over Gulf of Alaska/eastern North Pacific. However, the most statistically significant ΔV values are located over the EAM region as well as North America (Fig. 10a), including the upper-level trough and ridge from Figure 9. This corresponds to the anomalous divergence on the leeside of the Rockies (Fig. 10b). Despite the robust differences in this region, there is still substantial internal variability over the mid-latitude Pacific and/or the upper levels.

Lastly, we evaluated the influence of NASH on the EAM responses, visualized by taking the strong – weak EAM responses during strong western NASH events and subtracting by the strong – weak EAM responses during weak western NASH events (Figure 11), done for both observations (Fig. 11a-c) and the dry AGCM (Fig. 11d-f). The climatological biases of the dry AGCM are apparent, with Great Plains LLJ strengthening 10° northward from the observational strengthening (Fig. 11a,d). However, by considering these biases and comparing the NASH-modulated strong – weak EAM response (shaded contours) with the original strong – weak EAM response (no NASH considered, solid black contours), it is evident that strong western NASH modulation is comparable between observations and the dry AGCM, i.e. a strong western NASH amplifies the Great Plains LLJ strengthening signal, especially on the side closest to the Rockies. The dry AGCM generally simulates enhanced 500-250-hPa layer-averaged divergence in the Plains associated with the enhanced precipitation anomalies from observations (Fig. 11b,e). This suggests that dry dynamics in the AGCM may be sufficient to produce basic NASH-related modulation of EAM-forced patterns, such that the signs of the response are correct (see Supplementary Figure 2 for full strong – weak EAM response separated by western NASH strength as in Figure 2). Z250 patterns outside North America compare well to observations, but there are discrepancies in the dry AGCM representation of NASH modulation of Z250 over North America (Fig. 11c,f) that may limit its representation.

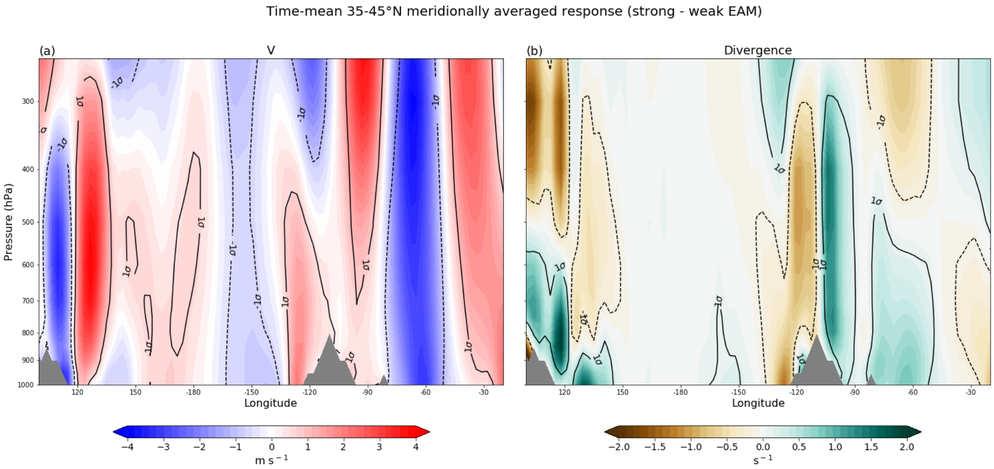

Figure 10. Subtraction difference between strong EAM experiment and weak EAM experiment 35-45°N meridionally averaged time-mean profile of (a) V and (b) divergence. The 1σ (solid black) and -1σ (dashed black) contours are overlaid as in Fig. 8.

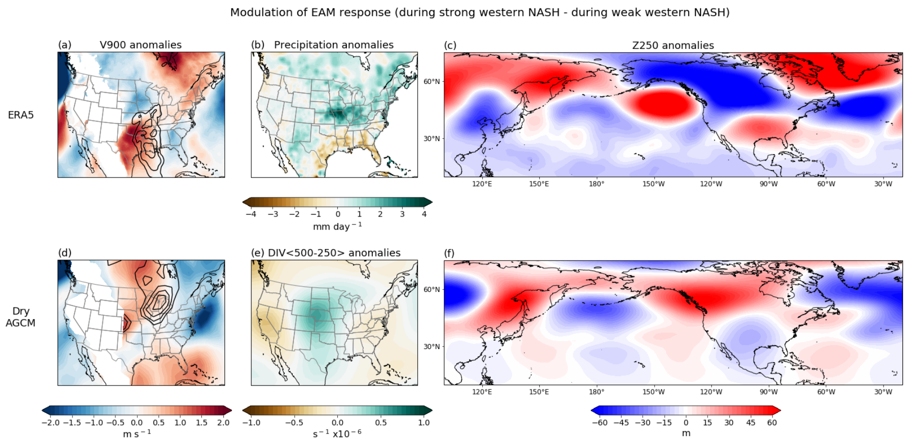

Figure 11. Modulation of EAM response by NASH: (a-c) Subtraction difference between ERA5 strong – weak EAM composites during strong western NASH and weak western NASH, i.e. Fig. 2g-i minus Fig. 2d-f. (d-f) Subtraction difference between strong EAM experiment – weak EAM experiment, i.e. strong – weak EAM response during strong western NASH minus strong – weak EAM response during weak western NASH, with 500-250-hPa layer-averaged divergence anomalies instead of precipitation anomalies. Strong – weak EAM V900 anomalies without NASH condition in Great Plains LLJ region are overlaid for left column for reference.

NASH modulation is further demonstrated by taking vertical profiles of meridional wind where the Great Plains LLJ strengthening occurs (averaged 25-30°N for observations and averaged 35-45°N for dry AGCM; Figure 12). NASH modulation of circulation is notably similar to observations and the dry AGCM except over North Atlantic. Over the region of interest that affects the Great Plains LLJ, the dry AGCM presents alignment of positive meridional wind values from the low to upper levels (Fig. 12b), though not as vertically stacked as presented in observations (Fig. 12a) or Figure 3. Overall, the dry AGCM simulates NASH modulation of EAM-forced responses to a reasonable degree, including the amplification of Great Plains LLJ strengthening and related divergence during strong EAM and strong western NASH events.

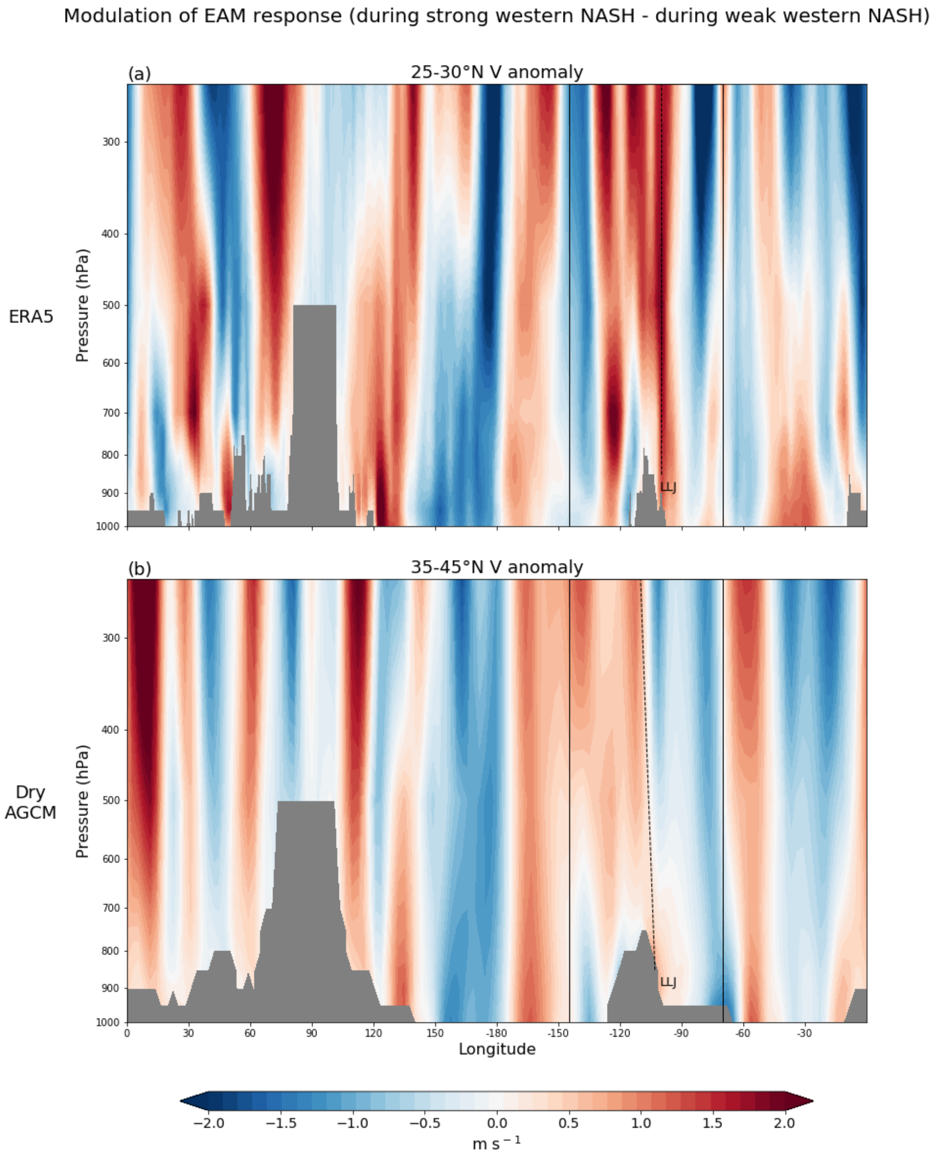

Figure 12. Modulation of vertical profile of EAM response by NASH: (a) Subtraction difference between ERA5 strong – weak EAM 25-30°N V composites during strong western NASH and weak western NASH. (b) Subtraction difference between strong EAM experiment – weak EAM experiment, i.e. strong – weak EAM 35-45°N V response during strong western NASH minus strong – weak EAM 35-45°N V response during weak western NASH. Each panel annotates the approximate location of the Great Plains LLJ, and a thin vertical dotted line from LLJ is displayed to visualize upper-level support.

4 Summary and Discussion

Seasonal forecasts of CONUS precipitation during the summer have relatively low skill, and there is little consensus on the driving causes of rainfall variability on this timescale. We suggest that examining large-scale Great Plains LLJ responses in observations and a dry nonlinear AGCM will aid in discerning dynamic causes and variability of pluvial events. First, we compared observational analysis of the NASH and EAM teleconnections and their interactions. Then we analyzed and compared Great Plains LLJ responses from EAM experiments in a dry AGCM and explored whether NASH modulation of EAM circulation responses can be reproduced with simple dry dynamics.

Results from the ERA5 conditional difference composites (Figure 1 and Figure 2) suggested that the strength of the western NASH or EAM matters when considering Great Plains LLJ impacts. Strong western NASH-related Great Plains LLJ strengthening and associated wet anomalies were greater during strong EAM events. However, EAM-related Great Plains LLJ responses were more dependent on the NASH location: during weak western NASH events, the strong – weak EAM response is a weakened Great Plains LLJ, and the LLJ response during strong western NASH events is not statistically significant. Profiles of meridional wind anomalies revealed that strong (weak) EAM and strong (weak) western NASH events were linked to in-phase lower- and upper-level circulation patterns, providing enhanced upper-level support for the Great Plains LLJ (Figure 3).

The strong – weak EAM responses were largely captured by the dry AGCM, including an elongated wave structure over the North Pacific and anomalous trough over western North America (Figure 9) comparable to observations (cf. Figure 2c). This promoted robust Great Plains LLJ strengthening (Figure 8). In addition, the dry AGCM simulated the amplification of the EAM-forced LLJ and mid- to upper-level divergence during a strong western NASH due to constructive interference of low- and upper-level wind patterns (Figures 10 and 11), shedding light on the major dynamic causes of Great Plains LLJ strengthening and its impacts.

Despite the AGCM capturing many of the dynamical processes behind EAM responses and NASH modulation, there were climatological biases in the AGCM that help explain some of the discrepancies between observations and the model's EAM-NASH-LLJ relationships. For example, in the upper levels, the model had a northward-shifted jet stream corresponding to increased horizontal height gradients further north (cf. Figure 4). Accordingly, the AGCM's Great Plains LLJ climatological core (Figure 5) and anomalies as well as the NASH were shifted northward. Our results complement previous research that found that the inaccurate location and strength of large-scale atmospheric features, such as the jet stream and subtropical high systems, can negatively impact long-range forecast skill (Y. Liu et al., 2019; O'Reilly et al., 2018) or change the associated primary rainfall patterns (W. Zhou et al., 2021). Biases or discrepancies between the observations and AGCM could also be from processes not represented in the model, like SST variability, land-atmosphere feedbacks, or moisture processes. For example, NASH modulation of Z250 patterns over North America was not as well represented in the dry AGCM as the rest of the domain (cf. Figure 11); this may indicate that ENSO variability is important to simulate NASH modulation over the continent (Malloy & Kirtman, 2022) or soil moisture-circulation feedbacks (Dirmeyer et al., 2003; Koster et al., 2006; Jong et al., 2021).

Previous studies have suggested that monsoon forcing is related to the circumglobal teleconnection (CGT), a prominent mode of upper-level height variability in the summer (Ding & Wang, 2005; Ding et al., 2011; S. Zhao et al., 2018). Typically, the CGT wavenumber-5 pattern is maintained by Indian monsoon heating, but F. Zhou et al. (2020) suggested the EAM influences the CGT. Agrawal et al. (2021) suggested that the CGT greatly influences May Great Plains LLJ activity. The study found that the CGT is dynamically linked to both coupled and uncoupled LLJ via an enhanced geostrophic flow from the upper-level wave pattern modulation. Additionally, Indian monsoon heating may relate to NASH shifts (Kelly & Mapes, 2011, 2013). While our results show similar features that relate the summer EAM to the CGT (F. Zhou et al., 2020) as well as the summer CGT to the Great Plains LLJ, it is beyond the scope of this study to diagnose and disentangle true causal relationships between the EAM, NASH, Indian monsoon, and CGT. Future work will be needed to understand these inter-relationships and how they contribute to rainfall variability over Asia, North America, and Europe.

A future study should expand on NASH's role by forcing vorticity anomalies over the western NASH region with the AGCM or investigating other sources of North Atlantic Rossby wave activity, e.g. NAO (Weaver & Nigam, 2008). In addition, the seasonal transition from early summer to late summer may also change the relationships between the NASH, EAM, and Great Plains LLJ. Simple AGCMs have the potential to isolate circulation responses from distinct forcing and evaluate the predictability of summer hydroclimate features. This research serves as a preliminary step for understanding more complex models and assessing the predictability of atmospheric dynamics in the summer on the more "elusive" long-range timescale.

5 Open Research

5.1 Data Availability Statement

All data in this study is available online. ERA5 data can be accessed through their website `https://www.ecmwf.int/en/forecasts/datasets/reanalysis-datasets/era5` (Hersbach et al., 2020). The CPC Global Unified Gauge-based Analysis data was provided by the NOAA PSL, Boulder, Colorado, USA, from their website at `https://psl.noaa.gov` (Chen et al., 2008; Xie et al., 2007). The dry AGCM and the model data from the article are available upon request.

Acknowledgments

The authors would like to acknowledge that this work was supported through NOAA Grants NA15OAR4320064, NA16OAR4310141, N16OAR4310149 and NA20OAR430472 and DOE Grant DE-SC0019433.

References

Agrawal, S., Ferguson, C. R., Bosart, L., & Burrows, D. A. (2021). Teleconnections governing the interannual variability of great plains low-level jets in may. *Journal of Climate*, *34*(12), 4785–4802.

Algarra, I., Eiras-Barca, J., Miguez-Macho, G., Nieto, R., & Gimeno, L. (2019, 2). On the assessment of the moisture transport by the great plains low-level jet. *Earth System Dynamics*, *10*, 107-119. doi: 10.5194/esd-10-107-2019

Arcodia, M. C., & Kirtman, B. P. (2022). Using simplified linear and nonlinear models to assess enso-modulated mjo teleconnections. *Climate Dynamics*.

Arritt, R. W., Rink, T. D., Segal, M., Todey, D. P., Clark, C. A., Mitchell, M. J., & Labas, K. M. (1997). The great plains low-level jet during the warm season of 1993. *Monthly Weather Review*, 2176-2192.

Banta, R. M., Newsom, R. K., Lundquist, J. K., Pichugina, Y. L., Coulter, R. L., & Mahrt, L. (2002). Nocturnal low-level jet characteristics over kansas during cases-99. *Boundary Layer Meteorology*.

Becker, E., den Dool, H. V., & Zhang, Q. (2014). Predictability and forecast skill in nmme. *Journal of Climate*, *27*, 5891-5906. doi: 10.1175/JCLI-D-13-00597.1

Beverley, J. D., Woolnough, S. J., Baker, L. H., Johnson, S. J., & Weisheimer, A. (2019, 3). The northern hemisphere circumglobal teleconnection in a seasonal forecast model and its relationship to european summer forecast skill. *Climate*

Dynamics, *52*, 3759-3771. doi: 10.1007/s00382-018-4371-4

Beverley, J. D., Woolnough, S. J., Baker, L. H., Johnson, S. J., Weisheimer, A., & O'Reilly, C. H. (2021, 11). Dynamical mechanisms linking indian monsoon precipitation and the circumglobal teleconnection. *Climate Dynamics*, *57*, 2615-2636. doi: 10.1007/s00382-021-05825-6

Blackadar, A. K. (1957). Boundary layer wind maxima and their significance for the growth of nocturnal inversions. *Bulletin of the American Meteorological Society*, *38*(5), 283–290.

Brenner, S. (1984). *The afgl global spectral model : expanded resolution baseline version* (Tech. Rep.). AIR FORCE GEOPHYSICS LAB HANSCOM AFB MA.

Burgman, R. J., & Jang, Y. (2015). Simulated u.s. drought response to interannual and decadal pacific sst variability. *Journal of Climate*, *28*, 4688-4705. doi: 10.1175/JCLI-D-14-00247.1

Byerle, L. A., & Paegle, J. (2003, 8). Modulation of the great plains low-level jet and moisture transports by orography and large-scale circulations. *Journal of Geophysical Research: Atmospheres*, *108*. doi: 10.1029/2002jd003005

Chen, M., Shi, W., Xie, P., Silva, V. B., Kousky, V. E., Higgins, R. W., & Janowiak, J. E. (2008, 2). Assessing objective techniques for gauge-based analyses of global daily precipitation. *Journal of Geophysical Research Atmospheres*, *113*. doi: 10.1029/2007JD009132

Cook, K. H., Vizy, E. K., Launer, Z. S., & Patricola, C. M. (2008). Springtime intensification of the great plains low-level jet and midwest precipitation in gcm simulations of the twenty-first century. *Journal of Climate*, *21*, 6321-6340. doi: 10.1175/2008JCLI2355.1

Danco, J. F., & Martin, E. R. (2018, 8). Understanding the influence of enso on the great plains low-level jet in cmip5 models. *Climate Dynamics*, *51*, 1537-1558. doi: 10.1007/s00382-017-3970-9

Ding, Q., & Wang, B. (2005). Circumglobal teleconnection in the northern hemisphere summer. *Journal of Climate*, *18*(17), 3483–3505.

Ding, Q., Wang, B., Wallace, J. M., & Branstator, G. (2011, 4). Tropical-extratropical teleconnections in boreal summer: Observed interannual variability. *Journal of Climate*, *24*, 1878-1896. doi: 10.1175/2011JCLI3621.1

Dirmeyer, P. A., Fennessy, M. J., & Marx, L. (2003). Low skill in dynamical prediction of boreal summer climate: Grounds for looking beyond sea surface temperature. *Journal of Climate*, *16*(6), 995–1002.

Fast, J., & McCorcle, M. (1990). A two-dimensional numerical sensitivity study of the great plains low-level jet. *Monthly Weather Review*, *118*, 151-164.

Feng, Z., Leung, L. R., Hagos, S., Houze, R. A., Burleyson, C. D., & Balaguru, K. (2016). More frequent intense and long-lived storms dominate the springtime trend in central us rainfall. *Nature communications*, *7*(1), 1–8.

García-Martínez, I. M., & Bollasina, M. A. (2020, 5). Sub-monthly evolution of the caribbean low-level jet and its relationship with regional precipitation and atmospheric circulation. *Climate Dynamics*, *54*, 4423-4440. doi: 10.1007/s00382-020-05237-y

Gianotti, D., Anderson, B. T., & Salvucci, G. D. (2013). What do rain gauges tell us about the limits of precipitation predictability? *Journal of Climate*, *26*, 5682-5688. Retrieved from `http://dx.doi.org/10.1175/JCLI-D-12-` doi: 10.1175/JCLI-D-12

Gimeno, L., Dominguez, F., Nieto, R., Trigo, R., Drumond, A., Reason, C. J., … Marengo, J. (2016, 10). Major mechanisms of atmospheric moisture transport and their role in extreme precipitation events. *Annual Review of Environment and Resources*, *41*, 117-141. doi: 10.1146/annurev-environ-110615-085558

Hao, Z., Singh, V. P., & Xia, Y. (2018, 3). Seasonal drought prediction: Advances, challenges, and future prospects. *Reviews of Geophysics*, *56*, 108-141. doi: 10.1002/2016RG000549

Harding, K., & Snyder, P. (2015). The relationship between the pacific–north american teleconnection pattern, the great plains low-level jet, and north central u.s. heavy rainfall events. *Journal of Climate*, *28*, 6729-6742.

He, J., Soden, B. J., & Kirtman, B. (2014). The robustness of the atmospheric circulation and precipitation response to future anthropogenic surface warming. *Geophysical Research Letters*, *41*(7), 2614–2622.

Hersbach, H., Bell, B., Berrisford, P., Hirahara, S., Horányi, A., Muñoz-Sabater, J., ... Thépaut, J. N. (2020, 7). The era5 global reanalysis. *Quarterly Journal of the Royal Meteorological Society*, *146*, 1999-2049. doi: 10.1002/qj.3803

Higgins, R. W., Yao, Y., Yarosh, E. S., Janowiak, J. E., & Mo, K. C. (1997). Influence of the great plains low-level jet on summertime precipitation and moisture transport over the central united states. *Journal of Climate*, 481-507.

Hodges, D., & Pu, Z. (2019, 4). Characteristics and variations of low-level jets in the contrasting warm season precipitation extremes of 2006 and 2007 over the southern great plains. *Theoretical and Applied Climatology*, *136*, 753-771. doi: 10.1007/s00704-018-2492-7

Holton, J. R. (1967, 1). The diurnal boundary layer wind oscillation above sloping terrain. *Tellus*, *19*, 200-205. doi: 10.3402/tellusa.v19i2.9766

Hu, Q., & Feng, S. (2012, 10). Amo- and enso-driven summertime circulation and precipitation variations in north america. *Journal of Climate*, *25*, 6477-6495. doi: 10.1175/JCLI-D-11-00520.1

Hu, Z.-Z., Kumar, A., Jha, B., & Huang, B. (2020, 2). How much of monthly mean precipitation variability over global land is associated with sst anomalies? *Climate Dynamics*, *54*, 701-712. doi: 10.1007/s00382-019-05023-5

Jha, B., Kumar, A., & Hu, Z. Z. (2019, 12). An update on the estimate of predictability of seasonal mean atmospheric variability using north american multi-model ensemble. *Climate Dynamics*, *53*, 7397-7409. doi: 10.1007/s00382-016-3217-1

Jiang, X., Lau, N. C., Held, I. M., & Ploshay, J. J. (2007, 2). Mechanisms of the great plains low-level jet as simulated in an agcm. *Journal of the Atmospheric Sciences*, *64*, 532-547. doi: 10.1175/JAS3847.1

Jong, B. T., Ting, M., & Seager, R. (2021, 3). Assessing enso summer teleconnections, impacts, and predictability in north america. *Journal of Climate*, *34*, 3629-3643. doi: 10.1175/JCLI-D-20-0761.1

Kam, J., Sheffield, J., Yuan, X., & Wood, E. F. (2014). Did a skillful prediction of sea surface temperatures help or hinder forecasting of the 2012 midwestern us drought? *Environmental Research Letters*, *9*(3), 1–9. doi: 10.1088/1748-9326/9/3/034005

Kelly, P., & Mapes, B. (2011). Zonal mean wind, the indian monsoon, and july drying in the western atlantic subtropics. *Journal of Geophysical Research Atmospheres*, *116*(D21), 1–16. doi: 10.1029/2010JD015405

Kelly, P., & Mapes, B. (2013). Asian monsoon forcing of subtropical easterlies in the community atmosphere model: Summer climate implications for the western atlantic. *Journal of Climate*, *26*, 2741-2755. doi: 10.1175/JCLI-D-12-00339.1

Kirtman, B. P., Paolino, D. A., Iii, J. L. K., & Straus, D. M. (2001). Impact of tropical subseasonal sst variability on seasonal mean climate simulations. *Monthly Weather Review*, *129*, 853-868.

Koster, R. D., Sud, Y., Guo, Z., Dirmeyer, P. A., Bonan, G., Oleson, K. W., ... others (2006). Glace: the global land–atmosphere coupling experiment. part i: overview. *Journal of Hydrometeorology*, *7*(4), 590–610.

Krishnamurthy, L., Vecchi, G. A., Msadek, R., Wittenberg, A., Delworth, T. L., & Zeng, F. (2015, 6). The seasonality of the great plains low-level jet and enso relationship. *Journal of Climate*, *28*, 4525-4544. doi: 10.1175/JCLI-D-14-00590.1

Lau, K.-M., & Weng, H. (2002). Recurrent teleconnection patterns linking summertime precipitation variability over east asia and north america. *Journal of the Meteorological Society of Japan. Ser. II*, *80*(6), 1309–1324.

Lee, S. K., Wang, C., & Mapes, B. E. (2009, 1). A simple atmospheric model of the local and teleconnection responses to tropical heating anomalies. *Journal of Climate*, *22*, 272-284. doi: 10.1175/2008JCLI2303.1

Li, L., Li, W., & Kushnir, Y. (2012, 9). Variation of the north atlantic subtropical high western ridge and its implication to southeastern us summer precipitation. *Climate Dynamics*, *39*, 1401-1412. doi: 10.1007/s00382-011-1214-y

Li, W., Li, L., Fu, R., Deng, Y., & Wang, H. (2011). Changes to the north atlantic subtropical high and its role in the intensification of summer rainfall variability in the southeastern united states. *Journal of Climate*, *24*(5), 1499–1506.

Liu, A. Z., Ting, M., & Wang, H. (1998). Maintenance of circulation anomalies during the 1988 drought and 1993 floods over the united states. *Journal of the Atmospheric Sciences*, *55*, 2810-2832.

Liu, Y., Ke, Z., & Ding, Y. (2019, 12). Predictability of east asian summer monsoon in seasonal climate forecast models. *International Journal of Climatology*, *39*, 5688-5701. doi: 10.1002/joc.6180

Lopez, H., Lee, S. K., Dong, S., Goni, G., Kirtman, B., Atlas, R., & Kumar, A. (2019, 6). East asian monsoon as a modulator of u.s. great plains heat waves. *Journal of Geophysical Research: Atmospheres*, *124*, 6342-6358. doi: 10.1029/2018JD030151

Mallakpour, I., & Villarini, G. (2016, 6). Investigating the relationship between the frequency of flooding over the central united states and large-scale climate. *Advances in Water Resources*, *92*, 159-171. doi: 10.1016/j.advwatres.2016.04.008

Malloy, K., & Kirtman, B. P. (2020, 2). Predictability of midsummer great plains low-level jet and associated precipitation. *Weather and Forecasting*, *35*, 215-235. doi: 10.1175/WAF-D-19-0103.1

Malloy, K., & Kirtman, B. P. (2022). The summer asia–north america teleconnection and its modulation by enso in community atmosphere model, version 5 (cam5). *Climate Dynamics*, 1–18.

Mariotti, A., Baggett, C., Barnes, E. A., Becker, E., Butler, A., Collins, D. C., ... Albers, J. (2020, 5). Windows of opportunity for skillful forecasts subseasonal to seasonal and beyond. *Bulletin of the American Meteorological Society*, *101*, E608-E625. doi: 10.1175/BAMS-D-18-0326.1

Mestas-Nuñez, A. M., Enfield, D. B., & Zhang, C. (2007, 5). Water vapor fluxes over the intra-americas sea: Seasonal and interannual variability and associations with rainfall. *Journal of Climate*, *20*, 1910-1922. doi: 10.1175/JCLI4096.1

Mitchell, M., Arritt, R., & Labas, K. (1995). A climatology of the warm season great plains low-level jet using wind profiler observations. *Weather and Forecasting*, *10*, 576-591.

Nayak, M. A., & Villarini, G. (2017, 2). A long-term perspective of the hydroclimatological impacts of atmospheric rivers over the central united states. *Water Resources Research*, *53*, 1144-1166. doi: 10.1002/2016WR019033

Nieto Ferreira, R., & Rickenbach, T. M. (2020). Effects of the north atlantic subtropical high on summertime precipitation organization in the southeast united states. *International Journal of Climatology*, *40*(14), 5987–6001.

O'Reilly, C. H., Woollings, T., Zanna, L., & Weisheimer, A. (2018, 8). The impact of tropical precipitation on summertime euro-atlantic circulation via a circumglobal wave train. *Journal of Climate*, *31*, 6481-6504. doi: 10.1175/JCLI-D-17-0451.1

Parish, T., Rodi, A., & Clark, R. (1988). A case study of the summertime great plains low level jet. *Monthly Weather Review*, *116*, 94-105.

Parish, T. R., & Oolman, L. D. (2010, 8). On the role of sloping terrain in the forcing of the great plains low-level jet. *Journal of the Atmospheric Sciences*, *67*, 2690-2699. doi: 10.1175/2010JAS3368.1

Patricola, C. M., Chang, P., & Saravanan, R. (2015, 4). Impact of atlantic sst and high frequency atmospheric variability on the 1993 and 2008 midwest floods: Regional climate model simulations of extreme climate events. *Climatic Change*, *129*, 397-411. doi: 10.1007/s10584-013-0886-1

Pegion, P. J., & Kumar, A. (2010, 8). Multimodel estimates of atmospheric response to modes of sst variability and implications for droughts. *Journal of Climate*, *23*, 4327-4341. doi: 10.1175/2010JCLI3295.1

Pu, B., & Dickinson, R. E. (2014). Diurnal spatial variability of great plains summer precipitation related to the dynamics of the low-level jet. *Journal of the Atmospheric Sciences*, *71*, 1807-1817. doi: 10.1175/JAS-D-13-0243.1

Pu, B., Dickinson, R. E., & Fu, R. (2016). Dynamical connection between great plains low-level winds and variability of central gulf states precipitation. *Journal of Geophysical Research: Atmospheres*, *121*(7), 3421–3434.

Schubert, S. D., Suarez, M. J., Pegion, P. J., & Kistler, M. A. (2002). Predictability of zonal means during boreal summer. *Journal of Climate*, *15*, 420-434.

Schubert, S. D., Wang, H., & Suarez, M. (2011, 9). Warm season subseasonal variability and climate extremes in the northern hemisphere: The role of stationary rossby waves. *Journal of Climate*, *24*, 4773-4792. doi: 10.1175/JCLI-D-10-05035.1

Shapiro, A., Fedorovich, E., & Rahimi, S. (2016, 8). A unified theory for the great plains nocturnal low-level jet. *Journal of the Atmospheric Sciences*, *73*, 3037-3057. doi: 10.1175/JAS-D-15-0307.1

Slater, L. J., Villarini, G., & Bradley, A. A. (2019). Evaluation of the skill of north-american multi-model ensemble (nmme) global climate models in predicting average and extreme precipitation and temperature over the continental usa. *Climate dynamics*, *53*(12), 7381–7396.

Tang, Y., Winkler, J., Zhong, S., Bian, X., Doubler, D., Yu, L., & Walters, C. (2017). Future changes in the climatology of the great plains low-level jet derived from fine resolution multi-model simulations. *Scientific reports*, *7*(1), 1–10.

Tian, D., Wood, E., & Yuan, X. (2017, 3). Cfsv2-based sub-seasonal precipitation and temperature forecast skill over the contiguous united states. *Hydrology and Earth System Sciences*, *21*, 1477-1490. doi: 10.5194/hess-21-1477-2017

Ting, M., & Wang, H. (1997). Summertime u.s. precipitation variability and its relation to pacific sea surface temperature. *Journal of Climate*, *10*, 1853-1873.

Ting, M., & Wang, H. (2006). The role of the north american topography on the maintenance of the great plains summer low-level jet. *Journal of the Atmospheric Sciences*, *63*, 1056-1068.

Trenberth, K., & Guillemot, C. (1996). Physical processes involved in the 1988 drought and 1993 floods in north america. *Journal of Climate*, *9*, 1288-1298.

Veres, M. C., & Hu, Q. (2013, 1). Amo-forced regional processes affecting summertime precipitation variations in the central united states. *Journal of Climate*, *26*, 276-290. doi: 10.1175/JCLI-D-11-00670.1

Wang, B., Wu, R., & Lau, K.-M. (2001). Interannual variability of the asian summer monsoon: Contrasts between the indian and the western north pacific-east asian monsoons. *Journal of Climate*, *14*, 4073-4090.

Wang, C. (2007, 9). Variability of the caribbean low-level jet and its relations to climate. *Climate Dynamics*, *29*, 411-422. doi: 10.1007/s00382-007-0243-z

Weaver, S. J., Baxter, S., & Harnos, K. (2016). Regional changes in the interannual variability of u.s. warm season precipitation. *Journal of Climate*, *29*, 5157-5173. doi: 10.1175/JCLI-D-14-00803.1

Weaver, S. J., & Nigam, S. (2008, 4). Variability of the great plains low-level jet: Large-scale circulation context and hydroclimate impacts. *Journal of Climate*, *21*, 1532-1551. doi: 10.1175/2007JCLI1586.1

Weaver, S. J., & Nigam, S. (2011, 1). Recurrent supersynoptic evolution of the great plains low-level jet. *Journal of Climate*, *24*, 575-582. doi: 10.1175/2010JCLI3445.1

Weaver, S. J., Ruiz-Barradas, A., & Nigam, S. (2009, 10). Pentad evolution of the 1988 drought and 1993 flood over the great plains: An narr perspective on the atmospheric and terrestrial water balance. *Journal of Climate*, *22*, 5366-5384. doi: 10.1175/2009JCLI2684.1

Weaver, S. J., Schubert, S. D., & Wang, H. (2009, 10). Warm season variations in the low-level circulation and precipitation over the central united states in observations, amip simulations, and idealized sst experiments. *Journal of Climate*, *22*, 5401-5420. doi: 10.1175/2009JCLI2984.1

Wei, W., Li, W., Deng, Y., & Yang, S. (2019, 7). Intraseasonal variation of the summer rainfall over the southeastern united states. *Climate Dynamics*, *53*, 1171-1183. doi: 10.1007/s00382-018-4345-6

Whiteman, C. D., Bian, X., & Zhong, S. (1997). Low-level jet climatology from enhanced rawinsonde observations at a site in the southern great plains. *Journal of Applied Meteorology*, *36*, 1363-1376.

Xie, P., Yatagai, A., Chen, M., Hayasaka, T., Fukushima, Y., Liu, C., & Yang, S. (2007, 6). A gauge-based analysis of daily precipitation over east asia. *Journal of Hydrometeorology*, *8*, 607-626. doi: 10.1175/JHM583.1

Yu, L., Zhong, S., Winkler, J. A., Doubler, D. L., Bian, X., & Walters, C. K. (2017, 1). The inter-annual variability of southerly low-level jets in north america. *International Journal of Climatology*, *37*, 343-357. doi: 10.1002/joc.4708

Zhao, G., Huang, G., Wu, R., Tao, W., Gong, H., Qu, X., & Hu, K. (2015). A new upper-level circulation index for the east asian summer monsoon variability. *Journal of Climate*, *28*, 9977-9996. doi: 10.1175/JCLI-D-15-0272.1

Zhao, S., Deng, Y., & Black, R. X. (2018, 12). An intraseasonal mode of atmospheric variability relevant to the u.s. hydroclimate in boreal summer: Dynamic origin and east asia connection. *Journal of Climate*, *31*, 9855-9868. doi: 10.1175/JCLI-D-18-0206.1

Zhou, F., Ren, H. L., Hu, Z. Z., Liu, M. H., Wu, J., & Liu, C. Z. (2020, 1). Seasonal predictability of primary east asian summer circulation patterns by three operational climate prediction models. *Quarterly Journal of the Royal Meteorological Society*, *146*, 629-646. doi: 10.1002/qj.3697

Zhou, S., L'Heureux, M., Weaver, S., & Kumar, A. (2012, 4). A composite study of the mjo influence on the surface air temperature and precipitation over the continental united states. *Climate Dynamics*, *38*, 1459-1471. doi: 10.1007/s00382-011-1001-9

Zhou, W., Leung, L. R., Song, F., & Lu, J. (2021). Future changes in the great plains low-level jet governed by seasonally dependent pattern changes in the north atlantic subtropical high. *Geophysical Research Letters*, *48*(4), e2020GL090356. Retrieved from `https://agupubs.onlinelibrary.wiley.com/doi/abs/10.1029/2020GL090356` (e2020GL090356 2020GL090356) doi: https://doi.org/10.1029/2020GL090356

Zhu, Z., & Li, T. (2016). A new paradigm for continental u.s. summer rainfall variability: Asia-north america teleconnection. *Journal of Climate*, *29*, 7313-7327. doi: 10.1175/JCLI-D-16-0137.1

Zhu, Z., & Li, T. (2018, 5). Amplified contiguous united states summer rainfall variability induced by east asian monsoon interdecadal change. *Climate Dynamics*, *50*, 3523-3536. doi: 10.1007/s00382-017-3821-8

Supplementary Material

Supplementary Table 1: List of months that went into Figure 1 and 2 difference composites, with red (blue) font color distinguishing between El Niño (La Niña) months defined by the Oceanic Niño Index (ONI) centered around previous month (e.g. June linked with April-May-June ONI value). No color indicates neutral ENSO conditions.

	Weak EAM	**Strong EAM**
Weak NASH	6/1979, 6/1981, 7/1981, 6/1997, 7/2000, 7/2004, 6/2005, 8/2006, 8/2007, 7/2008, 6/2009, 8/2011, 6/2012	8/1979, 7/1980, 6/1983, 7/1983, 7/1984, 7/1987, 6/1988, 6/1995, 8/1998, 7/2005, 7/2007, 8/2008
Strong NASH	7/1988, 6/1990, 7/1994, 8/1994, 8/1997, 7/2002, 6/2004, 8/2004, 6/2013, 7/2017, 6/2018, 7/2018, 8/2018	7/1986, 7/1991, 7/1992, 8/1993, 7/1996, 6/1998, 6/2000, 7/2003, 8/2003, 6/2015, 6/2016, 7/2019

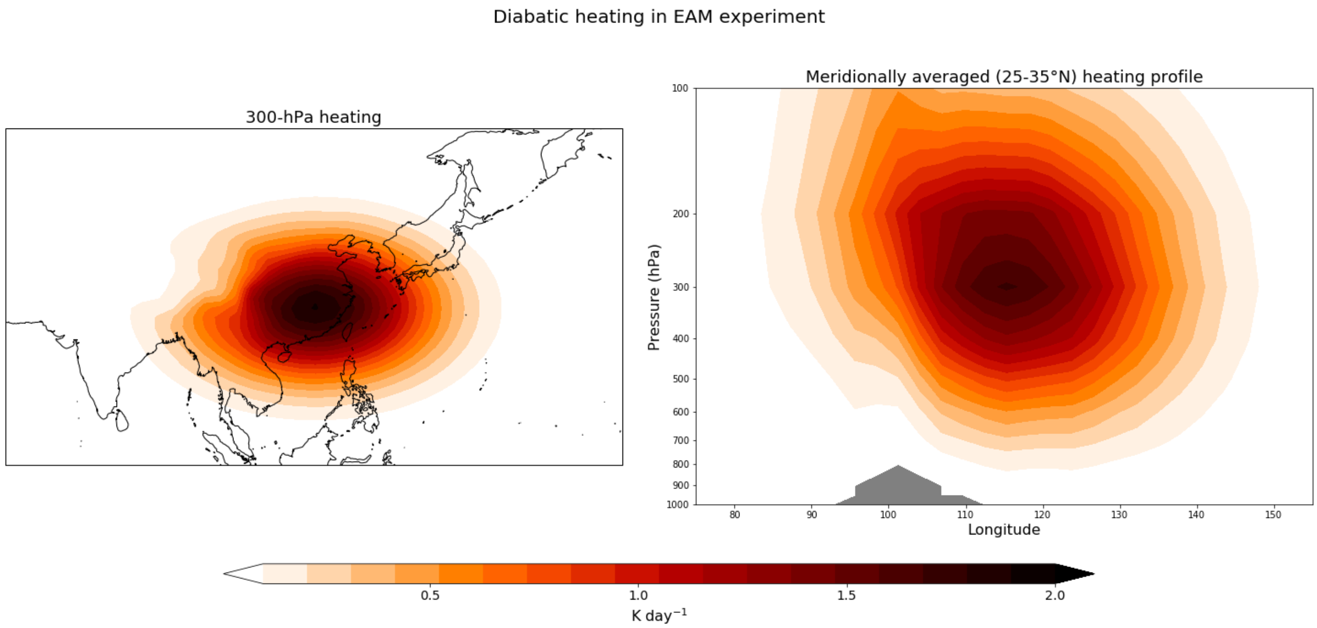

Supplementary Figure 1: Diabatic heating in strong EAM experiment (left) at 300 hPa and (right) meridionally averaged between 25°N and 35°N. Weak EAM experiment has equivalent structure, but of the opposite sign (negative diabatic heating).

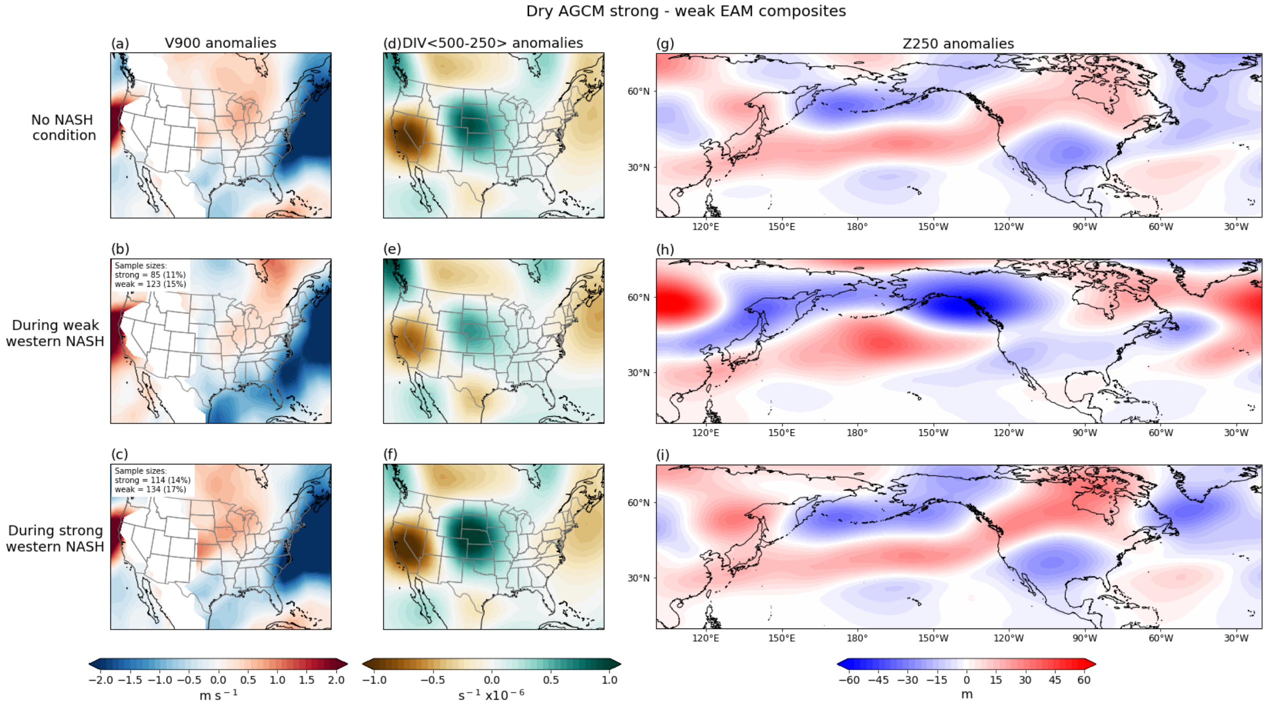

Supplementary Figure 2: Same format as Fig 2, but with 500-250-hPa layer-averaged divergence anomalies instead of precipitation anomalies.